Differential Interferometric Measurement of Instability in a Hypervelocity Boundary Layer

N. J. Parziale[1] and J. E. Shepherd[2] and H. G. Hornung[3]

California Institute of Technology, Pasadena, CA, 91125

I. Introduction

The prediction of laminar-turbulent transition location in high-speed boundary layers is critical to hypersonic vehicle design, because of the weight implications of increased skin friction and surface heating rate after transition. Current work in T5 (Caltech's free piston reflected shock tunnel) includes the study of problems relevant to hypervelocity boundary layer transition on cold wall slender bodies. With the ability to ground-test hypervelocity flows, the study of energy exchange between the boundary layer instability and the internal energy of the fluid is emphasized. The most unstable mode on a cold wall slender body is not the viscous instability (as in low speed boundary layers), but the acoustic instability [1, 2]. Quantitative characterization of this disturbance is paramount to the development of transition location prediction tools.

Traditionally, fast response piezo-electric pressure transducers, heat flux gauges, or hot wire anemometry techniques are used in this type of study [3–5]; however, the high frequency and small wavelength of the disturbances render these techniques inadequate above 1 MHz for conditions in T5. Recently, time-resolved visualization of the acoustic instability at moderate reservoir enthalpy (3-4 MJ/kg) has been reported[6]. That study utilized a dual-field-lens schlieren system with an extended light source, which was used to reduce the depth of focus of the system in order to reduce the contribution of disturbances outside of the boundary layer; however, even at the high frame rate (500 kHz) available, the exposure time (500 ns) is too long to adequately capture the

---

[1] Ph.D. Student, GALCIT, 1200 E. California Blvd. MC 205 45. AIAA Student Member
[2] Professor, GALCIT, 1200 E. California Blvd. MC 205 45. AIAA Member
[3] Emeritus Professor, GALCIT, 1200 E. California Blvd. MC 205 45. AIAA Fellow

acoustic instability at the boundary layer edge velocities of the current work in T5. Resonantly enhanced focused schlieren work in T5 has yielded some promising results [7]. Peaks in the spectral content at frequencies consistent with the acoustic instability were found along with detection of turbulent bursts; however, the method of resonantly enhanced focused schlieren makes quantitative interpretation of the results difficult.

This technical note describes a quantitative non-intrusive optical scheme that is used to investigate disturbances in a hypervelocity boundary layer on a five degree half-angle cone. The technique, focused laser differential interferometry (FLDI), has been successfully implemented to make quantitative measurements of density perturbations with high temporal (25 MHz) and spatial (700 μm) resolution. The acoustic instability is detected, with a peak in the spectral response at over 1 MHz. The experimental setup and results are presented and future plans are discussed.

II.   Experimental Setup

All experiments are performed in T5, the reflected shock tunnel at the California Institute of Technology. T5 is a facility designed to simulate high–enthalpy real gas effects on the aerodynamics of vehicles flying at high speed through the atmosphere. In all experiments the test article is a one meter long, five degree half angle aluminum cone, and the test gas is air. Focused two beam differential interferometry (FLDI) is the measurement technique applied in the present work (Fig. 1). This method was first applied to gas-dynamics by Smeets and George at the French-German Research Institute of Saint-Louis (ISL) in the 1970's [8–10]. To measure the acoustic instability on a slender body in a large scale reflected shock tunnel (such as T5), five requirements of the diagnostic are clear: 1) high temporal resolution of the measurement technique ($>$10 MHz), 2) high spatial resolution to capture the small wavelength of the disturbance ($<$1 mm), 3) insensitivity to mechanical vibration, 4) the capability to have a small focal volume near the surface of the cone, and 5) a straightforward and repeatable means of extracting quantitative data from the technique. These requirements are met with FLDI. Bench-tests of the span-wise response of the current FLDI to a subsonic CO_2 jet were made to assess the focusing ability of the technique; it was found that the 1/e folding length of the response in the span-wise direction to a continuous disturbance is

approximately ± 10 mm [11]. Additionally, the FLDI is used to measure the free-stream density fluctuations in T5 [11].
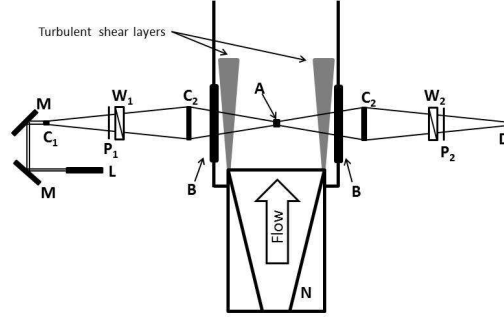
Fig. 1 Annotated schematic of the FLDI. L, Laser; M, mirror; C, lens; P, polarizer; W, Wollaston prism; B, window; A, probe volume; D, photodetector; N, nozzle.

The laser used in this experiment is a Spectra-Physics Excelsior diode pumped solid state continuous wave laser (532 nm wavelength, 200 mW power). The high quality beam (TEM_{00}) does not require additional beam conditioning for use as an interferometer. Following the optical path in Fig. 1, starting from the laser, the beam is turned by a periscope arrangement for precise directional control. The beam is expanded by a lens, C_1, and linearly polarized by P_1 at $45°$ to the plane of separation of the first Wollaston prism, W_1. The plane of separation of W_1 is chosen to be parallel to streamlines in the boundary layer of the five degree half angle cone. The prism splits the light by a narrow angle (2 arc minutes) into orthogonally polarized beams. The separation of the beams is fixed at 350 μm by a lens, C_2, while the diameter of the beams is reduced to small values in the center of the test section. This arrangement creates two beams with orthogonal polarization that share much of the same optical path. The orthogonally polarized beams do not share the same optical path within ± 10 mm of the focal point (along the beam direction, centered at A in Fig. 1). In this region the beams are calculated to be less than 100 μm in diameter, and traverse separate but very closely spaced volumes; they are 350 μm apart (assuming $1/e^2$ Gaussian beam propagation [12]). It is primarily within this small focal region that the diagnostic is sensitive to

changes in optical path length (OPL). The spatial resolution of the technique (700 μm) is set by doubling the beam spacing to satisfy the Nyquist sampling theorem. Beyond the beam focus, the optical paths are again common and an additional lens, C_2, re-focuses the beams. The Wollaston prism, W_2, and polarizer, P_2, recombine and then mix the orthogonally polarized beams, such that the interference will be registered as irradiance fluctuations by the photodetector. The response of the photodetector (22.5V battery biased FDS100 photodiode) is amplified (SRS SR445) at a gain of 5 and digitized at 100MHz by a 14-bit Ethernet oscilloscope (Cleverscope CS328A-XSE).

A relation between the fluctuations in density and output voltage from the photodetector is used for post-processing. This relation is found by considering the region within ± 10 mm of the focal point, along the beam direction (where the optical paths are not common), to be a two beam differential interferometer. The technique detects differences in phase, primarily due to the density differences at the two spatially separated focal regions; thus, making the interferometer sensitive to spatial density differences in the stream-wise direction. The relation for change in phase to irradiance (due to change in OPL) is

$$I_d = I_1 + I_2 + 2\hat{l_1} \cdot \hat{l_2} \sqrt{I_1 I_2} cos(\Delta\phi), \tag{1}$$

where $\Delta\phi$ is the phase change at the beam focus, I_d is the irradiance at the detector's surface, and I_1 and I_2 are the irradiances of the orthogonally polarized beams. They are equal, $I_1 = I_2 = I_0$, and, after the beams are mixed by the second polarizer their unit vectors' dot product, $\hat{l_1} \cdot \hat{l_2}$, is unity. The change in phase is

$$\Delta\phi = \frac{2\pi}{\lambda_0}\Delta OPL \approx \frac{2\pi}{\lambda_0}L\Delta n, \tag{2}$$

where L is the integration length over the phase object in the focal region, Δn is the change in refractive index between the two beams, and λ_0 is the wavelength of the laser. From the Gladstone-Dale relationship,

$$n = K\rho + 1, \tag{3}$$

Eq. 2 becomes

$$\Delta\phi = \frac{2\pi}{\lambda_0}LK(\rho_\parallel - \rho_\perp) = \frac{2\pi}{\lambda_0}LK\Delta\rho. \tag{4}$$

4

The change in phase, $\Delta\phi$, is due to the difference in density, $\rho_\parallel - \rho_\perp = \Delta\rho$. The densities are the instantaneous local densities interrogated by the beams polarized parallel ($\rho_\parallel$) and orthogonal ($\rho_\perp$) to the streamlines in the boundary layer. The two beams are spaced 350 μm apart, and the phase object is integrated over the OPL, L (within ±10 mm of the focal point). The integration length over the phase object is determined by inspecting a lay-over (Fig. 2) of the calculated boundary layer thickness (performed by BLIMPK88) and calculated beam profile (assuming Gaussian beam propagation).
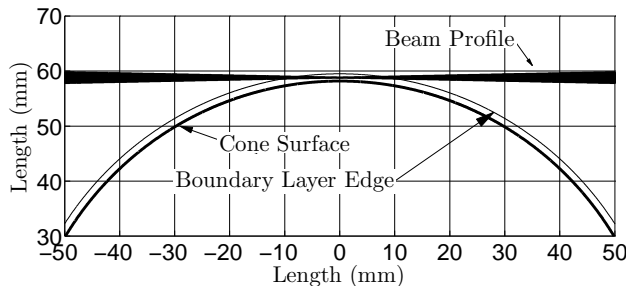
Fig. 2 Lay-over of the calculated boundary layer thickness (performed by BLIMPK88) and calculated beam profile (assuming Gaussian beam propagation)

For comparison between experiments it is more convenient to think of density changes in non-dimensional terms. Normalizing $\Delta\rho$ by the mean local density, ρ_L (calculated from BLIMPK88) makes Eq. 4,

$$\Delta\phi = \frac{2\pi}{\lambda_0} L K \rho_L \frac{\Delta\rho}{\rho_L}. \tag{5}$$

The potential response of the photodetector, V is expressed as

$$V = I\mathcal{R}R_L, \tag{6}$$

where $\mathcal{R}$ is the responsivity of the photodiode and R_L is the load resistance. A relation for the normalized change in density in terms of the output voltage of the photodetector and several fixed parameters in the experiment is found by combining Eqs. 1, 5 and 6 as

$$\frac{\Delta\rho}{\rho_L} = \frac{\lambda_0}{2\pi K L \rho_L} \sin^{-1}\left(\frac{V}{V_0} - 1\right). \tag{7}$$

The interferometer is set to the most linear part of a fringe before each experiment, so there is a $\pi/2$ rad phase shift introduced, and $V_0 = 2I_0\mathcal{R}R_L$. The phase shift, $\Delta\phi$ is less than $\pi/3$ rad, so

there is no fringe ambiguity. For all shots the volume being probed by the FLDI is 560 ±75 μm from the surface of the cone as measured with a Mitutoyo dial-indicator, translating a razor-blade cutoff normal to the surface of the cone. The distance from the cone tip is 665 ±5 mm or 783 ±5 mm measured with a conventional measuring tape.

### III.   Current Test Series and Results

The current shot series (see conditions in Table 1 computed by the codes ESTC and NENZF [13, 14]) was executed as a continuation of work for the transition delay project in T5 [15]. During these experiments, the FLDI technique was used to try to measure the disturbances in the boundary layer, the state of which is largely laminar at the measurement point (based on time-averaged heat flux correlations). Two examples (Fig. 3 and Fig. 4) are presented where both turbulent bursts and wave packets are detected; the spectral content estimation in these examples is obtained using Welch's method, with 50% overlapping 20 μs Hann windows.
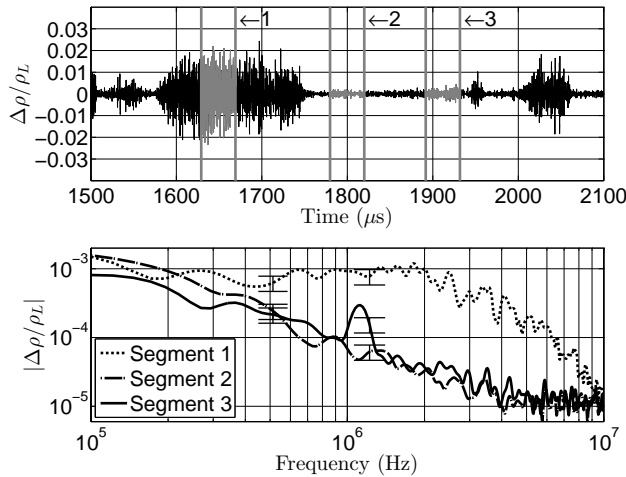
Fig. 3 FLDI Results from shot 2695, the processed response (top) and spectral response from the three chosen segments (bottom).

The FLDI response for shot 2695 (Fig. 3) reveals interesting phenomena at 1650 μs and 1915 μs; 40 μs segments centered at 1650 μs, 1800 μs, and 1915 μs are highlighted. This shows the spectral content of the interrogated point of the boundary layer when minimal disturbances are detected (Segment 2), when a turbulent spot passes (Segment 1), and when a wave packet passes (Segment

6

3). The spectral content of the turbulent spot (Segment 1) shows broadband response; the wave packet (Segment 3) has a strong peak in response at 1.11 MHz.
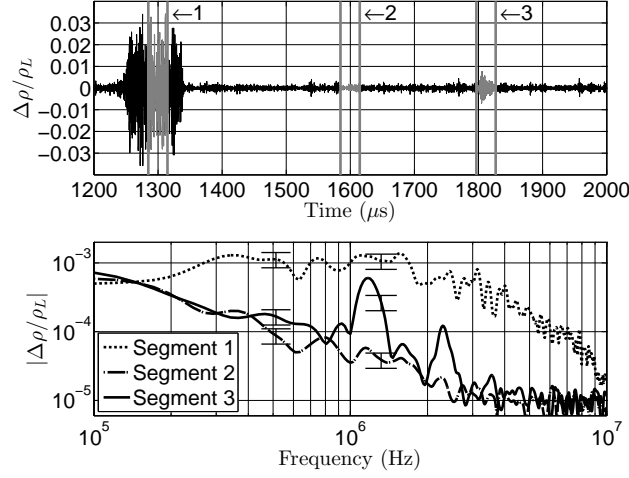
Fig. 4 FLDI Results from shot 2702, the processed response (top) and spectral response from the three chosen segments (bottom).

The FLDI response for shot 2702 (Fig. 4) reveals interesting phenomena at 1300 μs and 1810 μs; 30 μs segments centered at 1300 μs, 1600 μs, and 1810 μs are highlighted. This shows the spectral content of the interrogated point of the boundary layer when minimal disturbances are detected (Segment 2), when a turbulent spot passes (Segment 1), and when a wave packet passes (Segment 3). The spectral content of the turbulent spot (Segment 1) shows broadband response; the wave packet (Segment 3) has a strong peak in response at 1.17 MHz with a harmonic at 2.29 MHz. Zooming in (in time) on Segment 3 of Fig. 4 shows the wave packet in more detail (Fig. 5). The wave packet appears in the unprocessed and unfiltered trace (top), and is more prominent after the raw data are filtered and processed with Eq. 7 (bottom).

The boundary layer profiles for each of the shots in this test series are computed with the BLIMPK88 code (Boundary Layer Integral Matrix Procedure with Kinetics [16, 17]). This program provides the solution to the multicomponent, non-equilibrium boundary layer problem, typical of conditions available in T5. The purpose of finding these profiles is to compare the scaling of the most unstable frequency ($f_M \approx 0.8u_{edge}/(2\delta_{99})$) to the measured frequency [2, 3]. These results are summarized in Table 2, where the scaling for shots 2695 and 2702 can be found along with
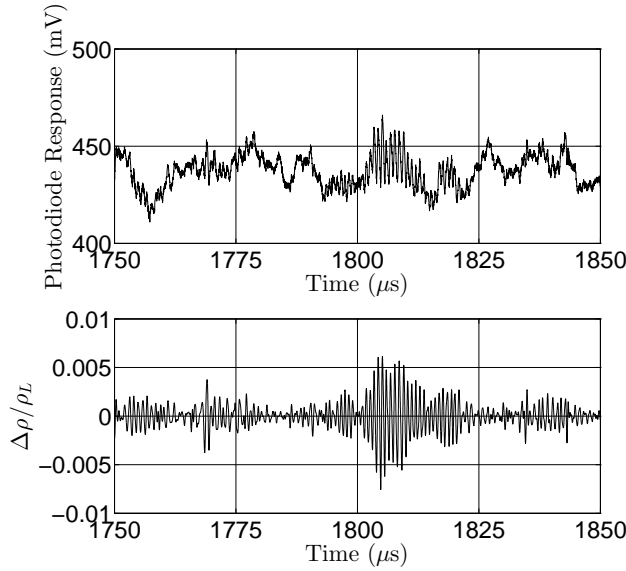
Fig. 5 FLDI Results from shot 2702, zoomed into Segment 3 of Fig. 4, showing the unprocessed photodetector response (top), and the data after they are filtered and processed with Eq. 7 (bottom).

other shots in which wave packets are detected. The interferometer was moved downstream for two experiments (shots 2704 and 2705). The purpose of doing so was to make measurements at approximately the same edge conditions (as shot 2702), but where the boundary layer is thicker; a thicker boundary layer at the same edge velocity should decrease the frequency of a wave packet measured at the probe volume. A decrease of between 10-15% in the peak measured frequency

Table 1 Run conditions for current shot series [a]

Shot	h_R (MJ/kg)	P_R (MPa)	u_∞ (m/s)	p_∞ (kPa)	T_∞ (K)	Re_∞^{unit} (1/m)
2695	7.15	48.4	3430	18.9	950	7.5e6
2696	7.26	46.0	3460	18.1	970	7.0e6
2697	8.66	49.3	3750	20.6	1230	5.7e6
2702	8.77	49.9	3770	21.0	1240	5.7e6
2704	8.72	49.5	3760	20.7	1240	5.7e6
2705	8.68	50.0	3750	20.9	1230	5.8e6

[a]h_R and P_R are the reservoir enthalpy and pressure. u_∞, p_∞, and T_∞ are the free-stream velocity, pressure, and temperature. Re_∞^{unit} is the unit Reynolds number based on the free-stream conditions.

(f_{peak}) is evident in Table 2.

The systematic error stemming from applying Eq. 7 to the raw data is found by considering the propagation of uncertainty in $\Delta\rho/\rho_L$ as a function of all the input parameters [18, 19]. The largest sources of systematic error are considered to be the uncertainty introduced by the assumed integration length, L in Eq. 2 (assumed to be 20%), the quantization error in the potentials, V and V_0 (assumed to be the 14-bit quantization error), and the magnitude of the local density ρ_L (assumed to be 20%). This leads to an error of approximately 20% in the magnitude of $\Delta\rho/\rho_L$, with a 95% confidence interval. There is systematic error in the magnitude of $\Delta\rho/\rho_L$ from the spectral content estimation in each of the segments, this is approximately 20% in the magnitude of $\Delta\rho/\rho_L$, with a 95% confidence interval. Combining the errors from processing the data and estimating their spectra in a root-mean-squared sense, the systematic error is bounded at 30% (95% confidence interval). This uncertainty is presented in the spectral content plots as error bars (bottom of Figs. 3 and 4).

Random error from electrical noise and mechanical vibrations can be estimated by inspecting the spectral content of the signal immediately preceding the test time. Approximately 10 ms before the test begins, vibration from the piston launch (to compress the driver gas) is transmitted through the steel rails the entire shock tunnel rests on. By applying the identical signal processing scheme

Table 2 Conditions at edge of boundary layer and peak frequency[a]

Shot	S_{meas} (mm)	p_{edge} (kPa)	T_{edge} (K)	u_{edge} (m/s)	δ_{99} (mm)	$0.8u_{edge}/(2\delta_{99})$ (MHz)	f_{peak} (MHz)
2695	665	28.0	1050	3400	1.23	1.11	1.11
2696	665	26.7	1070	3420	1.27	1.08	1.11
2697	665	29.7	1340	3720	1.32	1.13	1.12
2702	665	30.1	1360	3730	1.27	1.17	1.17
2704	783	29.9	1350	3730	1.43	1.07	0.98
2705	783	30.1	1360	3730	1.43	1.06	1.03

[a]S_{meas} is the distance from the cone tip to the measurement location. p_{edge}, T_{edge}, and u_{edge} are the pressure, temperature and velocity at the edge of the boundary layer. δ_{99} is the wall normal distance at which the stream-wise velocity is 99% of u_{edge}. f_{peak} is the measured peak frequency.

to the time just before the test, as used during the test, errors from ambient electrical noise and facility vibration can be bounded. In the 100 kHz to 10 MHz frequency band, the spectral content from vibration and electrical noise is less than 0.5% in the magnitude of $\Delta\rho/\rho_L$ (95% confidence interval).

Random error from the FLDI's imperfect focusing ability comes from the optical technique having to traverse the core flow and turbulent shear layer from the turbulent boundary layer on the nozzle wall (refer to Fig. 1). The core flow and turbulent shear layer could introduce additional noise to the measurement of the probe volume. The noise resulting from the fluctuations in the core flow and shear layer are bounded in frequency space by the spectral content of the quiescent windows of the signal as in Segment 2 of Fig. 3 and Fig. 4, where minimal disturbances are detected in the boundary layer. Using a two-tailed hypothesis test, it is found that there is a statistically significant difference between the response of the FLDI when minimal disturbances are present (Segment 2), and when a wave packet is detected (Segment 3) in the frequency range of the acoustic instability (99.999% confidence interval). Additionally, the signal to noise ratio of the peak (Segment 3/Segment 2) is at least 5 in Fig. 3, and is at least 10 in Fig. 4. We conclude that the noise floor that is a result of the shear layer and core flow is sufficiently low, so that the FLDI technique can resolve the acoustic instability.

IV. Conclusions and Future Work

The ability to make quantitative measurements of the acoustic instability with FLDI in a hypervelocity slender body boundary layer is reproducibly demonstrated. This is notable because of the time scales (1-3 MHz) associated with the acoustic instability's fundamental and harmonic frequency for conditions available in T5. The error and noise floor associated with the measurement technique (FLDI) and facility are sufficiently low that we propose to use an additional FLDI to be placed downstream of the current FLDI to make acoustic instability growth rate measurements.

by NASA/AFOSR National Center for Hypersonic Research in Laminar-Turbulent Transition, for which Dr. John Schmisseur is the program manager. The views and conclusions contained herein are those of the authors and should not be interpreted as necessarily representing the official policies or endorsements, either expressed or implied, of the Air Force Office of Scientific Research or the U.S. Government.

References

[1] Mack, L. M., "Linear Stability Theory and the Problem of Supersonic Boundary-layer Transition," *AIAA*, Vol. 13, No. 3, July 1975, pp. 278–289. doi: 10.2514/3.49693

[2] Federov, A., "Transition and Stability of High-Speed Boundary Layers," *Annual Review of Fluid Mechanics*, Vol. 43, August 2011, pp. 79–95. doi: 10.1146/annurev-fluid-122109-160750

[3] Stetson, K. and Kimmel, R. L., "On Hypersonic Boundary-layer Stability," *Proceedings of the 30th Aerospace Sciences Meeting*, AIAA-1992-737, Reno, NV, 1992.

[4] Tanno, H., Komura, T., Sato, K., Itoh, K., Takahashi, M., and Fujii, K., "Measurements of Hypersonic Boundary Layer Transition on Cone Models in the Free-Piston Shock Tunnel HIEST," *Proceedings of 47th AIAA Aerospace Sciences Meeting*, AIAA-2009-781, Orlando, FL, 2009.

[5] Heitmann, D., Kähler, C., Radespiel, R., Rödiger, T., Knauss, H., and Wagner, S., "Non-Intrusive Generation of Instability Waves in a Planar Hypersonic Boundary Layer," *Experiments in Fluids*, Vol. 50, August 2011, pp. 457–464. doi: 10.1007/s00348-010-0949-2

[6] Laurence, S. J., Wagner, A., Hannemann, K., Wartemann, V., Lüdeke, H., Tanno, H., and Itoh, K., "Time-Resolved Visualization of Instability Waves in a Hypersonic Boundary Layer," *AIAA*, Vol. 50, No. 6, 2012, pp. 243–246. doi: 10.2514/1.56987

[7] Parziale, N. J., Jewell, J. S., Shepherd, J. E., and Hornung, H. G., "Shock Tunnel Noise Measurement with Resonantly Enhanced Focused Schlieren Deflectometry," *Proceedings of the 28th International Symposium on Shock Waves*, ISSW, pp. 747-752, Manchester, UK, 2011.

[8] Smeets, G., "Laser Interferometer for High Sensitivity Measurements on Transient Phase Objects," *IEEE Transactions on Aerospace and Electronic Systems*, Vol. AES-8, No. 2, March 1972, pp. 186–190. doi: 10.1109/TAES.1972.309488

[9] Smeets, G. and George, A., "Laser Differential Interferometer Applications in Gas Dynamics," Translation of ISL Internal Report 28/73, Original 1975, Translated by A. Goetz, 1996.

[10] Smeets, G., "Flow Diagnostics by Laser Interferometry," *IEEE Transactions on Aerospace and Electronic*

Systems, Vol. AES-13, No. 2, March 1977, pp. 82–90. doi: 10.1109/TAES.1977.308441

[11] Parziale, N. J. and Shepherd, J. E. and Hornung, H. G., "Reflected Shock Tunnel Noise Measurement by Focused Differential Interferometry," *42nd AIAA Fluid Dynamics Conference*, AIAA-2012-3261, New Orleans, LA, 2012.

[12] Siegman, A. E., *Lasers*, University Science Books, 1986.

[13] Mcintosh, M. K., "A Computer Program for the Numerical Calculation of Equilibrium and Perfect Gas Cnditions in Shock Tunnels," Technical Report CPD 169, Australian Defense Scientific Service, 1969.

[14] Lordi, J., Mates, R. E., and Moselle, J. R., "Computer Program for the Numerical Solution of Nonequilibrium Expansions of Reacting Gas Mixtures," NASA CR-472, 1966.

[15] Jewell, J. S., Leyva, I. A., Parziale, N. J., and Shepherd, J. E., "Effect of Gas Injection on Transition in Hypervelocity Boundary Layers," *Proceedings of the 28th International Symposium on Shock Waves*, ISSW, pp. 735–740, Manchester, UK, 2011.

[16] Bartlett, E. P. and Kendall, R. M., "An Analysis of the Coupled Chemically Reacting Boundary Layer and Charring Ablator, Part III; Nonsimilar Solution of the Multicomponent Laminar Boundary Layer by an Integral Matrix Method," Aerotherm Final Report 66-7, Acurex Corporation, also NASA CR-1062, 1967.

[17] Tong, H., Buckingham, A. C., and Morse, H. L., "Nonequilibrium Chemistry Boundary Layer Integral Matrix Procedure," Aerotherm Final Report 73-67, Acurex Corporation, also NASA CR-134039, 1973.

[18] Kline, S. J. and McClintock, F. A., "Describing Uncertainties in Single Sample Experiments," *Mechanical Engineering*, Vol. 75, 1953, pp. 3–8.

[19] Beckwith, T. G., Marangoni, R. D., and Lienhard, J. H., *Mechanical Measurments*, Pearson-Prentice Hall, Sixth ed., 2007.